J Pathol Inform

Editor-in-Chief:
Anil V. Parwani , Columbus, OH, USA
Liron Pantanowitz, Pittsburgh, PA, USA

OPEN ACCESS
HTML format

For entire Editorial Board visit : www.jpathinformatics.org/editorialboard.asp

Research Article

Quantitative analysis of myocardial tissue with digital autofluorescence microscopy

Thomas Jensen[1], Henrik Holten-Rossing[1], Ida M H Svendsen[2], Christina Jacobsen[2], Ben Vainer[1]

[1]Department of Pathology, Rigshospitalet, University of Copenhagen, [2]Department of Forensic Pathology, University of Copenhagen, Copenhagen, Denmark

E-mail: *Dr. Thomas Jensen - thlj@dadlnet.dk
*Corresponding author

Received: 01 November 2015 Accepted: 23 February 2016 Published: 11 April 2016

Abstract

Background: The opportunity offered by whole slide scanners of automated histological analysis implies an ever increasing importance of digital pathology. To go beyond the importance of conventional pathology, however, digital pathology may need a basic histological starting point similar to that of hematoxylin and eosin staining in conventional pathology. This study presents an automated fluorescence-based microscopy approach providing highly detailed morphological data from unstained microsections. This data may provide a basic histological starting point from which further digital analysis including staining may benefit. **Methods:** This study explores the inherent tissue fluorescence, also known as autofluorescence, as a mean to quantitate cardiac tissue components in histological microsections. Data acquisition using a commercially available whole slide scanner and an image-based quantitation algorithm are presented. **Results:** It is shown that the autofluorescence intensity of unstained microsections at two different wavelengths is a suitable starting point for automated digital analysis of myocytes, fibrous tissue, lipofuscin, and the extracellular compartment. The output of the method is absolute quantitation along with accurate outlines of above-mentioned components. The digital quantitations are verified by comparison to point grid quantitations performed on the microsections after Van Gieson staining. **Conclusion:** The presented method is amply described as a prestain multicomponent quantitation and outlining tool for histological sections of cardiac tissue. The main perspective is the opportunity for combination with digital analysis of stained microsections, for which the method may provide an accurate digital framework.

Key words: Autofluorescence, digital pathology, histomorphometry

Access this article online

Website: www.jpathinformatics.org

DOI: 10.4103/2153-3539.179908

Quick Response Code:

BACKGROUND

Microscopic evaluation of myocardial tissue is commonly conducted at pathological and forensic departments, usually by means of bright-field microscopy of hematoxylin and eosin-stained (H and E) microsections. A part of the evaluation is a subjective estimate of the basic condition of the heart as perceived, e.g., amount of fibrosis, cell size, nuclear size, and presence of lipofuscin. In clinical settings, subjective estimates of histological

This article may be cited as:
Jensen T, Holten-Rossing H, Svendsen IM, Jacobsen C, Vainer B. Quantitative analysis of myocardial tissue with digital autofluorescence microscopy. J Pathol Inform 2016;7:15.

Available FREE in open access from: http://www.jpathinformatics.org/text.asp?2016/7/1/15/179908

parameters may work, but in scientific settings the need for reproducible parametric representation of data is not satisfied. Furthermore, with the current introduction of whole slide scanners in clinical settings, a demand for automated analysis of digitized microsections is increasingly manifested. This study explores the digital analysis of autofluorescence from unstained microsections as a means to quantitate basic histological parameters of myocardial tissue. The method is intended for both clinical and scientific purposes.

The versatility of autofluorescence is reflected in the broadness of previous application studies ranging from noninvasive methods for diagnosing cancer and metabolic diseases[1-4] to histological diagnostics of functional disorders.[5,6] The common feature is quantitation of tissue components and/or metabolites by means of fluorescent properties.

Methods for automated quantitation of histological tissue components in myocardial microsections using digital image analysis have been widely published.[7-14] Fibrous tissue has attracted a surplus of attention. Three principal approaches for quantitating fibrous tissue have been applied: (i) Discrimination by staining color, (ii) discrimination by polarization properties, and (iii) discrimination by fluorescence properties. Regarding (i) specific staining is necessary to provide robust detectable contrast in color, e.g., by Sirius red or Masson's trichrome staining.[8,9,14] Regarding (ii) it is well established that birefringence of Sirius-stained fibrous tissue is suitable for digital quantitation.[9,12] Regarding (iii) fibrous tissue has been quantitated with a combination of two-photon excitation of autofluorescence and second harmonic generation imaging of collagen,[7,11] which requires a confocal fluorescence microscope mounted with a femtosecond laser. This setup is limited in availability and has so far been tested only on experimentally acquired myocardial tissue.[7,11] In addition to fibrous tissue, cardiac lipofuscin has been the subject of autofluorescence-based quantitation,[10,13] specifically by discriminating lipofuscin with autofluorescence intensity.

In this study, we aimed to test autofluorescence as the base of an objective high-throughput method for quantitating the histological presentation of tissue structures in myocardial microsections. This was performed by quantitative analysis of histological autofluorescence intensities obtained at different wavelengths with a commercially available slide scanner. Settings for image acquisition along with quantitation algorithms are presented. The method quantitates both fibrous tissue, myocytes, lipofuscin, and the extracellular phase (ECP) in unstained microsections. In addition, the method was tested at various fixation times and microsection thicknesses as autofluorescence is known to increase with fixation time[15] and microsection thickness is expected to affect the autofluorescence.

METHODS

We identified twenty autopsies performed at the Pathology Department, Rigshospitalet, University of Copenhagen, Denmark, in the period 2009–2013 with archived samples of myocardial tissue. The regional ethics committee classified the study as a methodology study requiring no Ethical approval. Relatives had given consent to both clinical and scientific aspects of the autopsy. In all cases, sampling was from the left ventricle and with the intention of verifying an infarction. All samples included areas with infarction as well as areas with noninfarcted myocardial tissue with various amounts of fibrosis. The latter was used as a model tissue. The age range of the included was 35–77 years (median = 65 years), the male/female gender ratio 14/6, and the postmortem interval at autopsy 24–136 h (median = 68 h). For testing the impact of fixation time and microsection thickness, an additional sample was taken from the left ventricle of a 59-year-old male autopsied 48 h postmortem in 2015.

Tissue Handling

All samples were formalin fixated (neutral buffered 4% solution) and paraffin embedded following routine procedures. The duration of fixation was between 1 and 5 days. Microsections were cut at 4 μm thickness. The additional sample was parted in two and fixated for 1 and 4 days, respectively. Each part was cut in microsections of 2 and 8 μm thickness following paraffin embedding. All microsections for autofluorescence were kept in the dark with minimal exposure to light when handled, which included 45 min of drying at 45°C, paraffin dissolution by 2 × 15 min of xylene immersion and mounting of coverslips using xylene-based glue (Pertex, Histolab Products AB, Göteborg, Sweden). Upon drying, the sections were ready for autofluorescence imaging. Fluorescence images were acquired, and the microsections were immersed in xylene until loosening of the cover slips and finally Van Gieson (VG) stained using a standard protocol. Neighboring microsections were H and E-stained following standard protocol.

Scanning

Areas of normal myocardium without infarction were identified on the H and E-stained microsections. The autofluorescence of these areas in the neighboring unstained microsections were imaged at two wavelengths within the visible spectrum: The blue area (using a DAPI-filter, excitation λ =365 nm, emission λ =445) and the red area (using a Rhodamine filter, excitation λ =555 nm, emission λ =605 nm) using a Zeiss Axio Scan Z1 slide scanner (Zeiss, Oberkochen, Germany) with an light emitting diode (LED) illumination module (Zeiss Colibri II) and an Orca Flash 4.0 camera. Ring aperture contrast (RAC) focus mode was used for both coarse (×20 objective, 6 points per area) and fine

autofocus (×20 objective, onion skin mode with the parameter set to 0.1). Scanning was done with the ×20 objective and exposure times were 100 ms in the blue area and 200 ms in the red area. We selected these exposure times through testing as they produced ample and similar autofluorescence intensities from the myocytes. During the scanning, both wavelengths were photographed immediately in each tile position by photographing first the blue area and then the red area. A scanned area was typically 3 × 3 mm. Stitching, which is a built-in function of the Zeiss microscope software that smooths the transition between imaged tiles, was disabled to avoid manipulation at the tile borders.

Point Grid Counting

After VG-staining of the digitally quantitated microsections, random parts of the quantitated areas were imaged at ×100 magnification using a standard light microscope (Leica DM2000 LED, Leica Microsystems, Wetzlar, Germany) mounted with a charge-coupled devices camera, resulting in 1.2 × 1.2 mm images. A point grid was applied to these images with random offset using an ImageJ grid plugin (Wayne Rasband, NIH) with a spacing of approximately 50 μm, giving a total of approximately 450 counting points in each image. The spacing corresponds to a higher sampling intensity than the 100 μm spacing suggested in a previous publication.[8] By eye observation on screen, each counting point was determined as representing either fibrous tissue (stained red), ECP (unstained), or cells (stained yellow).

RESULTS AND ANALYSIS

The obtained autofluorescence images were in focus with level contrast and intensity. All images were considered suitable for further analysis. Examples are given in Figure 1. Particular differences between the two wavelengths are noted. In the blue filter [Figure 1a], the intensity of fibrous tissue was high and the intensity of lipofuscin was low. The opposite holds true for the red filter [Figure 1b]. The images can be regarded as different stainings simultaneously of one microsection. No bleaching artifacts from autofocus could be identified. The inserted intensity histograms include fitted standard deviations corresponding to the myocytes. In both wavelengths, they were considered normally distributed.

Image Analysis

In keeping with the objective high throughput commitment, it was considered mandatory to develop a reproducible quantitation algorithm suitable for fully automated processing. The quantitation algorithm was based on parametric data analysis of the autofluorescence intensities. In particular, the fibrous tissue was determined by analysis of pixel intensity ratios of blue-to-red autofluorescence, lipofuscin by analysis of pixel intensity ratios of red-to-blue autofluorescence, and ECP by analysis of pixel intensities of blue autofluorescence. The pixel intensity ratios are best appreciated as images. Figure 1c shows an image where pixel values are ratios of blue-to-red autofluorescence intensities from the

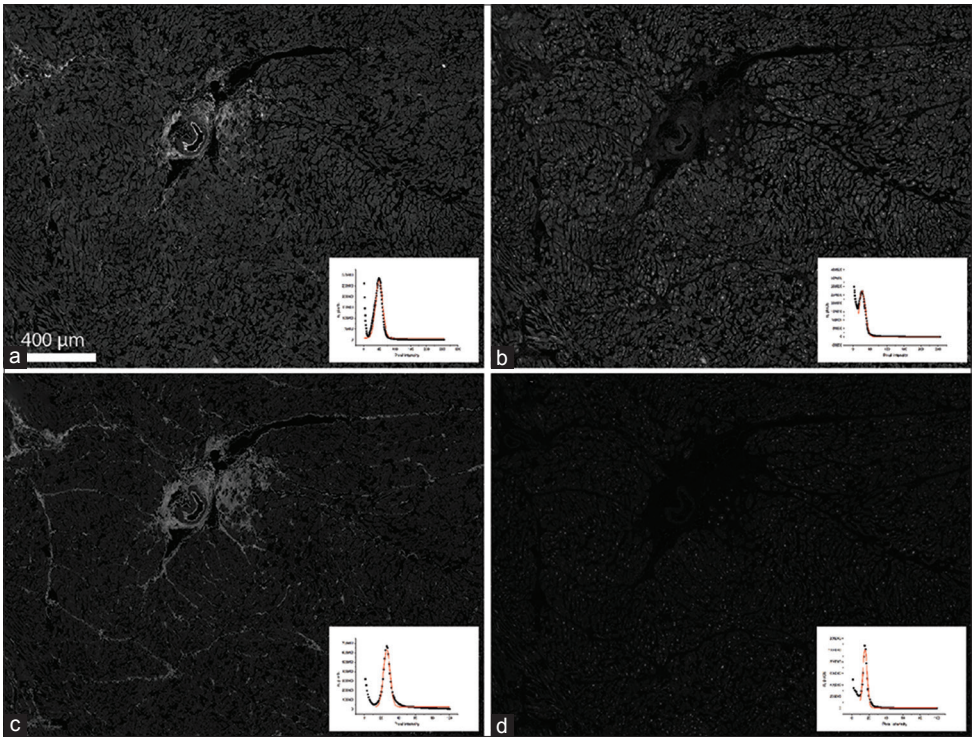

Figure 1: Examples of fluorescence images. (a and b) The same area in the blue and the red filter, respectively. (c and d) The corresponding ratio images with (c) being the ratio of blue to red and (d) the ratio of red to blue. Intensity histograms with fitted standard deviations corresponding to the myocyte peaks are shown in the small insets. Van Gieson-staining and quantitations of the central parts of this microsection are displayed in Figure 2

corresponding pixels in Figure 1a, b, and d show the reciprocal image consisting of red-to-blue ratios. In the blue-to-red ratio image [Figure 1c], the myocytes are seen as a featureless background with uniform intensity, whereas the fibrous tissue is amplified and leveled. In the red-to-blue ratio image [Figure 1d], lipofuscin is amplified and leveled.

All image analysis was done using ImageJ,[16] Origin (Origin Lab Corporation, Northampton, MA, USA) and Excel (Microsoft, Redmond, WA, USA). All images entered the analysis in 8-bit gray scale form.

The following Steps 1–5 present the autofluorescence-based quantitation, which has been tested on various area sizes. If the area is below 1 × 1 mm, the included fitting procedures become unstable due to irregular, "spikey" intensity histograms. If the area is too large, variations in the microsection thickness may theoretically provide instability. This problem, however, was not encountered analyzing bigger areas up to 3 × 3 mm. It is consequently recommended to perform the analysis on square sections of at least 1 × 1 mm and be cautious with squares more than 3 × 3 mm.

- Step 1: Creation of a mask of the ECP is performed using a standard distribution fitted to the myocyte peak in the histogram of the blue autofluorescence image. This was done by exporting the intensity histogram from ImageJ to Origin and fit a single peak in the fit module with Gauss function checked. Pixels with intensities below the fitted peak value-2 standard deviations are thresholded from the remaining image and used as a mask representing ECP [Figure 2]

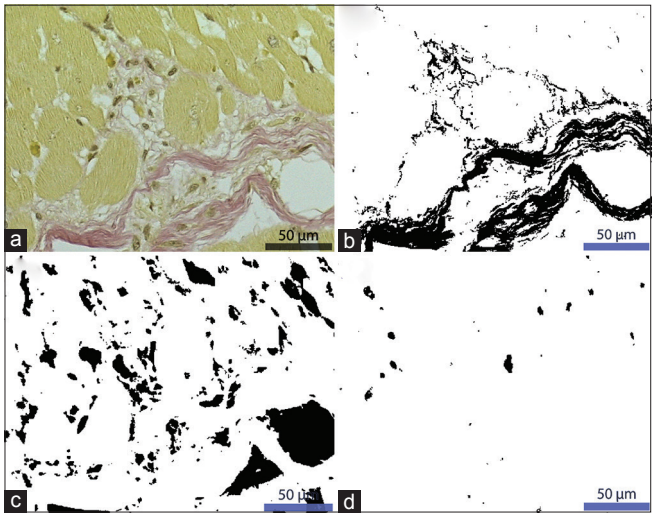

Figure 2: High magnification image of a Van Gieson-stained area (a) and the corresponding black/white masks from the digital quantitations including fibrous tissue (b), extracellular phase (c), and lipofuscin (d). This particular section was selected as both solid fibrous tissue with strands down to a few micrometers (lower half) as well as hardly discernible network-like strands below 1 µm (e.g. the capillarized area central left) are represented

- Step 2: The ECP mask is subtracted from the blue and the red images using the image calculator function in ImageJ resulting in ECP being represented with the value 0
- Step 3: The images are leveled with respect to the peak intensity of the myocytes: The blue/red ratio of the myocyte peak intensities is identified from histograms (Please see small insets in Panels a-b of Figure 1) and used to align the red with the blue image using the math → multiply function. For instance, the red image is multiplied by 2 if the myocyte peak intensity value of the blue image is twice that of the red image
- Step 4: Creation of a mask of the fibrous tissue by generating and analyzing the blue-to-red ratio image. In summary, the standard deviation (SD) of the myocyte peak in the ratio image is used to approximate the upper-intensity level that includes pixels covering myocytes, and a transition analysis is performed to reproducibly identify that particular level. In the case of the blue to red ratio image, fibrous tissue is considered all pixels with intensity above the upper intensity level of the myocytes, and in the case of the red-to-blue ratio image, lipofuscin is considered all pixels with intensity above the level of the myocytes. The detailed procedure for identifying fibrous tissue is described in the following: The blue image is divided with the red image using the image calculator function; 32-bit float must be checked. In the resulting ratio image, the intensity variation of all tissue elements is leveled, and the fibrous tissue intensity is amplified, and lipofuscin intensity is diminished. Typically, fibrous tissue is too small a representation to be represented by a peak in the intensity histogram of the generated ratio image [Figure 1c]. Hence, fibrous tissue must be defined based on the myocyte peak as follows: A standard distribution is fitted to the myocyte peak of the ratio image, which in theory is located at 1.0. By eye observation, it was established that the transition from myocytes to fibrous tissue is approximately at 5 SD above the myocyte peak intensity, where intensity values above represent fibrous tissue and intensities below represent myocytes. Thus, peak intensity + 5 SD is used as the starting point of the myocyte-to-fibrous tissue transition analysis. The transition analysis considers the drop in pixels covering myocytes as the threshold approaches the signal emanating from fibrous tissue. In particular, single pixel presentations are regarded as reminiscences of myocytes. All single-pixel representations above threshold are quantitated for each 0.02 threshold interval in the range: Starting point (myocyte peak intensity + 5 SD) ± 0.40, which covers approximately 10% of the intensity range of the generated 32-bit ratio image. The ratio of change in single pixel presentations to the number of single pixel presentation at the

initial point of the analysis ($\Delta n_{0.02}/n_{starting\ point\ -\ 0.40}$) is plotted against the intensities of the analyzed range. It is noted that the change in single pixel presentations approach zero with increasing threshold [Figure 3]. In the plots, an exponential equation approaching zero asymptotically is fitted using the function "fit exponential → asymptotic1" in origin [Figure 3]. The adjusted R^2 of the 20 fits performed in this study was typically around 0.95 and 0.88 at lowest. The fit provides the basis for selecting the threshold reproducibly, which was defined in this study as the intensity of the fit corresponding to the value $\Delta n/n_{starting\ point\ -\ 0.40} = -0.015$

- Step 5: Creation of a mask for lipofuscin is done by repeating step 4 only replacing the blue-to-red ratio with the red-to-blue ratio.

The output of the digital quantitation algorithm is best presented as black/white masks of the quantitated tissue components (black pixels) [Figure 2]. Regarding fibrous tissue [Figure 2b] and ECP [Figure 2c], differences between the VG-stained section and the autofluorescence-based digital quantitations are inconspicuous. Lipofuscin [Figure 2d] cannot be identified in the VG-stained section. The images are representative of all quantitations. The solid fibrous tissue is readily recaptured, whereas recapturing of the thin strands is less certain. The thin strands are probably in the proximity of the lower limit of what can be quantitated with the presented technique.

Verification of Digital Quantitations

This part of the results and analysis section concerns verification of the digital quantitations. The VG-stainings were used both for point grid counting for correlation with the digital quantitations and an analytical comparison between color depth and autofluorescence intensities.

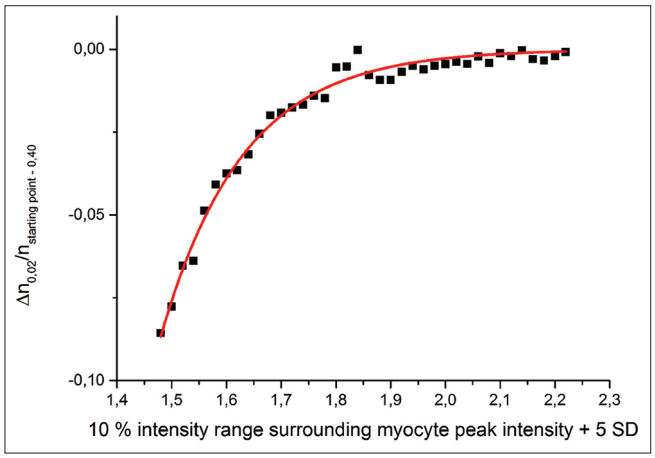

Figure 3: Transition analysis plot of drop in the ratio of change in single pixel presentations to the number of single pixel presentation at the initial point of the analysis ($\Delta n_{0,02}/n_{starting\ point\ -\ 0,40}$) plotted against the intensities of the analyzed range. The red line is an exponential fit asymptotically approaching zero

Figure 4a shows an example of a point grid quantitated area along with corresponding digital quantitation of ECP [Figure 4b], fibrous tissue [Figure 4c], and lipofuscin [Figure 4d]. Fibrous tissue, ECP, and cells were quantified in the point grid analysis. It was not possible to quantify lipofuscin using the VG-stain because the lipofuscin could not be differentiated from surrounding myocyte cytosol. Scatter plots displaying the correlations between point grid quantitations and digital quantitations are presented in Figure 5. The digital quantitation of cells is the entire area of the section with fibrous tissue and ECP subtracted. An evident correlation is noted. The function y = x is entirely included in confidence intervals of the cell and ECP quantitations. The confidence interval of the fibrous tissue quantitation is slightly below x = y in the central part of the fit corresponding to a small systematic underestimation of fibrous tissue in the digital quantitation.

As a further means to validate the digitally quantitated fibrous tissue and ECP, an analytical proof of concept is presented in Figures 6 and 7. In Figure 6, part of a VG-stained section is shown that includes strands of fibrous tissue. The red color corresponding to fibrous tissue is demarcated by including increasing intensities of the red spectrum using the RGB color threshold feature of ImageJ, where Figure 6d was set to fit the fibrous tissue as perceived by the author. Figure 6e-h show the same section of the blue-to-red ratio image, where pixels in Panels f-h are increasingly demarcated going from highest to lowest intensity with Panel h representing the digitally determined threshold. It is noted that deeper red in the VG staining corresponds to higher gray scale intensity of

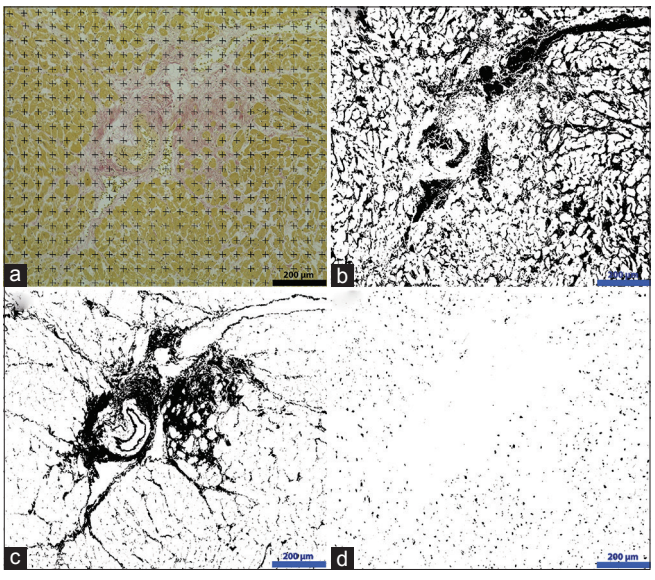

Figure 4: Panel (a) displays a Van Gieson-stained section with an superimposed point grid, whereas panels (b-d) displays outlines of the corresponding digital quantitations of extracellular phase, fibrous tissue, and lipofuscin, respectively. This particular section includes a higher amount of dispersive fibrous tissue than normal myocardium

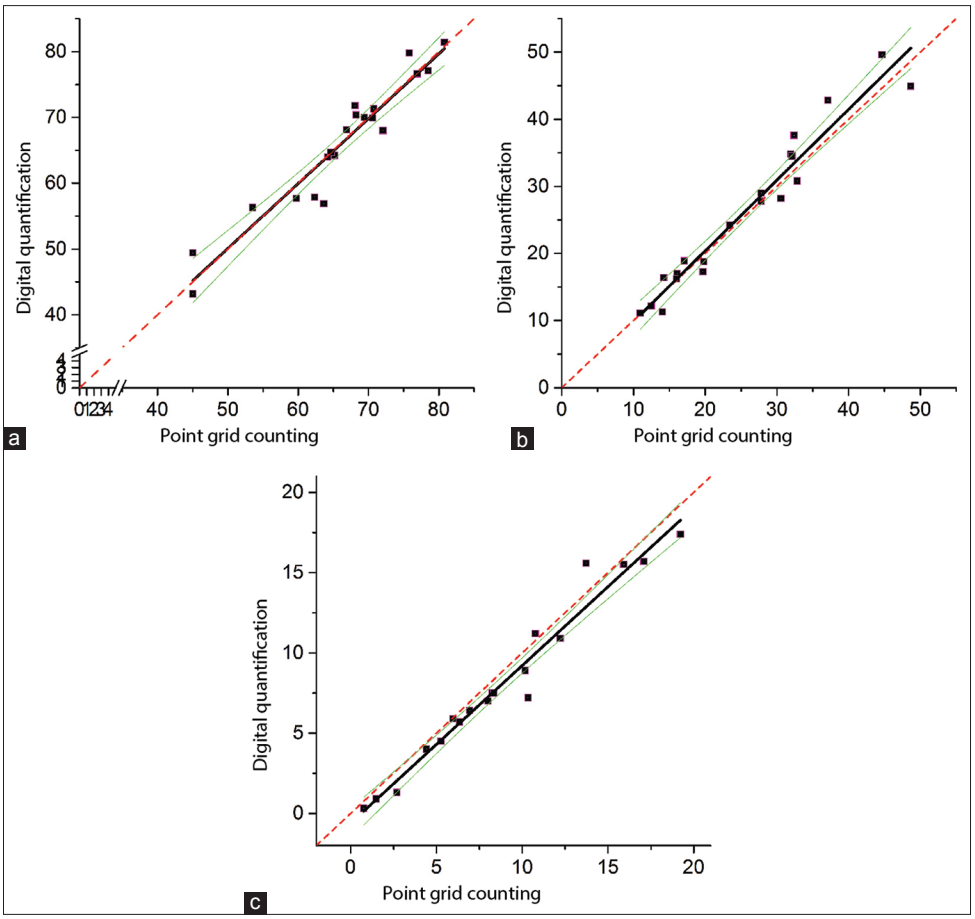

Figure 5: Scatterplots of point grid counting versus digital quantitations of cells (a), extracellular phase (b), and fibrous tissue (c). X = Y is added as a red dashed line, black full line is least squares fitted line, and the green lines display the 95% confidence intervals thereof

the ratio image. The area was chosen, as it includes solely fibrous tissue because myocytes in the VG-staining could not be digitally distinguished from fibrous tissue.

A similar approach was used for ECP. Figure 7 displays a VG-stained area [Figure 7a-d] along with the corresponding area in the blue autofluorescence image [Figure 7e-h]. In the VG-images, decreasing pixel intensities are demarcated resulting in the lightest areas of the section, which is regarded as ECP, being increasingly demarcated. In Figure 7d, the demarcation has been set to fit ECP as perceived by the author. In Panels e-h, increasing intensities are demarcated, with Panel h representing the digitally determined threshold. It is noted that the highest intensities of the VG-stained section correspond to the darkest pixels in the blue autofluorescence image. This analytical approach verifies the point grid quantitation by proving that the autofluorescence intensity, through quantitative analysis, correlates to the as-perceived fibrous tissue, and ECP of a VG-stained section.

As for verification of the lipofuscin quantitation, no comparison can be done to the VG-stained sections. Figure 8 shows an example of lipofuscin content analysis. Panel a is an autofluorescence image in the red area. The outline mask of the corresponding digitally quantitated lipofuscin is shown in Panel b. Panel c is panel a with a slightly translucent Panel b on top.

Impact of Fixation Time and Microsection Thickness

Microsections cut at 2 and 8 μm from samples fixated for 1 and 4 days, respectively, were digitally analyzed and quantified with point grid quantification as described above. Long fixation time as well as thicker microsections resulted in an overall higher autofluorescence intensity in both the blue and the red area. At both fixation times and both microsection thicknesses the digital quantitation algorithm was applied successfully with satisfying correlations to the point grid quantitations. The outer boundaries of this additional experiment were the thin microsections fixated for 1 day and the thick microsections fixated for 4 days, which had the lowest and highest impacts, respectively, of thickness and fixation time on autofluorescence. Close-up examples of these boundary samples with VG-staining and corresponding fibrous tissue quantitation are shown in Figure 9. Panels 9a-b is a thin microsection fixated for 1 day and 9c-d is

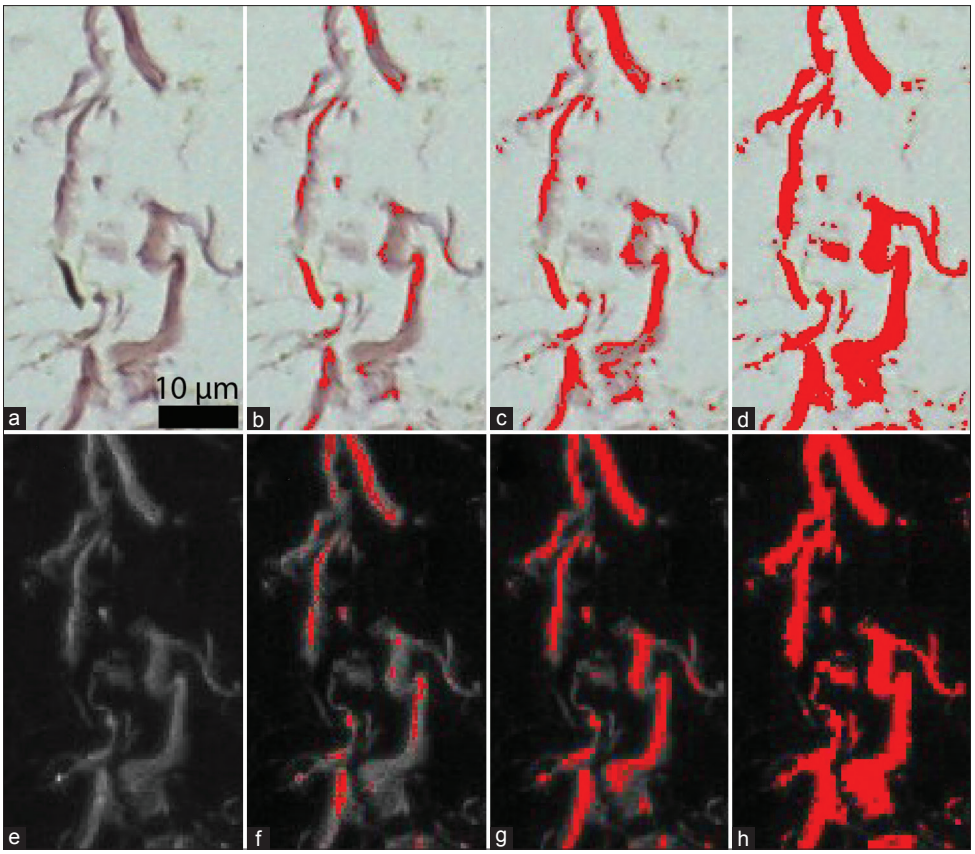

Figure 6: Images of the same section demonstrating the analytical verification of the fibrous tissue quantitation. In (a-d), which are Van Gieson-stained, increasing areas of red are demarcated with red going from deep red to lighter nuances of red. In (e-h), which is the blue to red ratio, image pixels with the highest intensity are demarcated in (f) and decreasing intensities are included toward (h) with (h) representing the digital quantitation

a thick microsection fixated for 4 days. The areas include transitions from solid fibrous tissue to hardly discernible smaller fibrils. As expected, the borders between stained and unstained components are unclear in the thick microsection (9c) compared to the thin microsection (9a). The fibrous tissue outline of the thin microsection (9b) is by inspection in clear correspondence with the VG-staining, whereas the outline of the thick section (9d) is in less obvious correspondence. This ambiguity was also present in thick microsections fixated for 1 day, but not in thin microsections fixated for 4 days. It should be noted that larger tissue component presentations were clearly outlined in the thick microsections.

DISCUSSION

We present an autofluorescence-based technique intended for quantitation of tissue components in histological sections of the myocardium. Unstained histological sections of archived tissue from autopsies were used. The study acknowledges autofluorescence intensity as a tissue property suitable for quantitation of tissue components in histological sections. The digital quantitations are verified by comparison to point grid counting performed on the same microsections VG-stained. The method separates itself from previous studies on digital quantitation of myocardial tissue components on two major points: (i) Several tissue components are quantitated from a single slide and (ii) no staining is required. The method may serve as a stand-alone part of any routine microscopic evaluation providing accurate quantitations and digital outlines of myocardial tissue components. This would provide immediate access to any desired distribution analysis of the microsection in question.

The quantitation algorithm is based on parametric analysis using no image manipulation such as contrast enhancing filtering. Although the approach provided satisfying quantitations in all cases, it is recognized that alternative analysis approaches may be applicable. In particular, filtering may replace the transition analysis, which would alleviate the computational strain. Using autofluorescence ratios for identifying tissue components, however, is considered indispensable for similar autofluorescence-based techniques. We recommend executing the algorithm on square areas of 1–3 mm in width.

The digital quantitations of fibrous tissue, ECP and myocytes were satisfyingly correlated to point grid

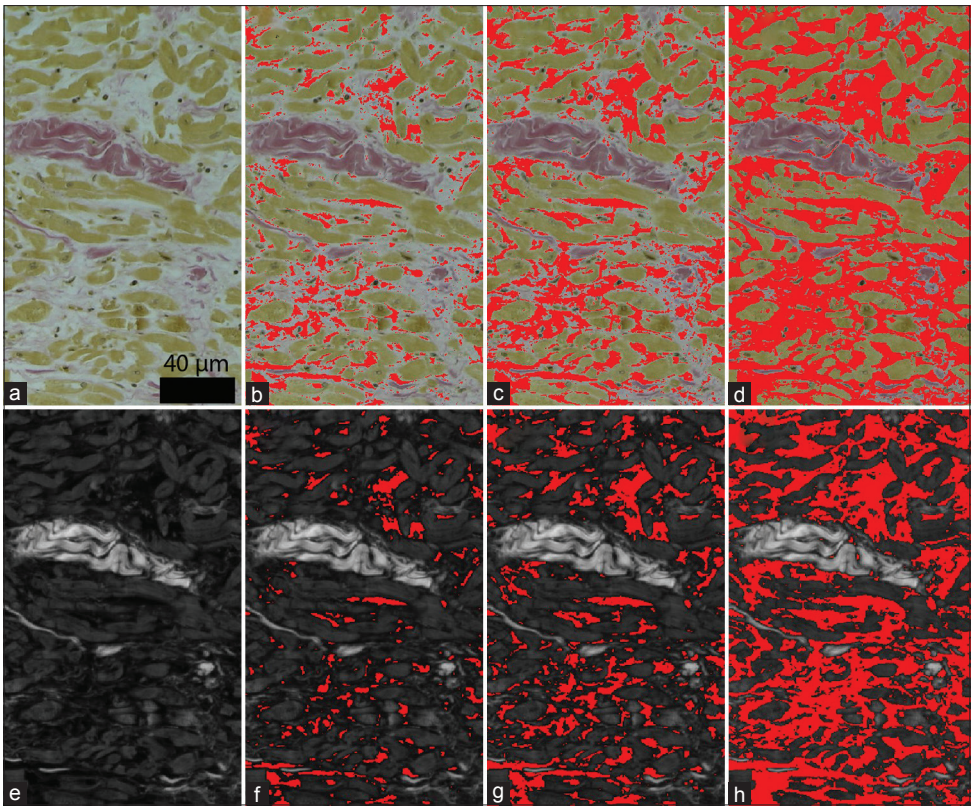

Figure 7: Images of a section demonstrating the analytical verification of the extracellular phase quantitation. In Panels a-d, which is Van Gieson-stained, areas of decreasing intensity are demarcated with red to cover the manually perceived extracellular phase completely (d). In the blue fluorescence image (e-h), areas of increasing intensity are demarcated with red with (h) representing the digital quantitation

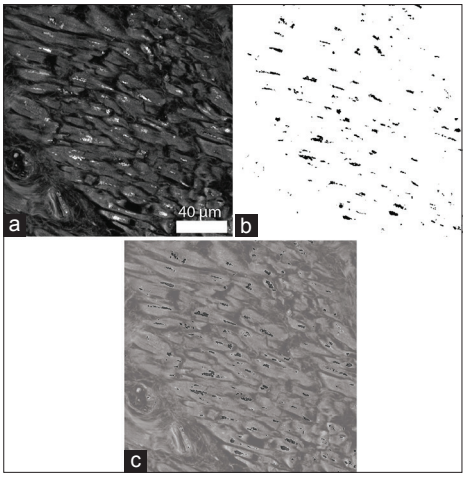

Figure 8: Depiction of the lipofuscin quantitation. Three images of the same section, where (a) is the autofluorescence image in the red area, (b) is the quantitated lipofuscin, and (c) is a combination of (a and b) with (b) made slightly translucent and layered on top of (a) for overview reasons

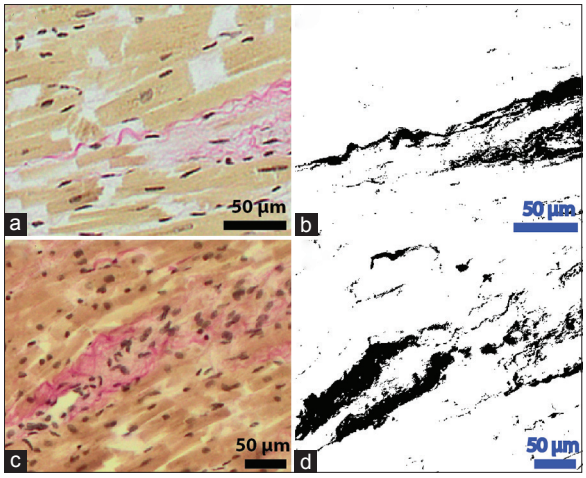

Figure 9: Examples from the additional study of the effect of microsection thickness and fixation time. Panel a is a thin (2 µm) microsection cut from the sample fixated for 1 day and Panel c is a thick microsection (8 µm) from the sample fixated for 4 days. Panel b and d are the corresponding outline masks of the digital quantitations of fibrous tissue. Panels a and b are representative of thin microsections fixated for 4 days and Panels c and d are representative of thick microsections fixated for 1 day

quantitations performed on the VG-staining. The digitally quantitated fibrous tissue, however, was marginally smaller than the point grid quantitation. A similar difference was noted in a previous study comparing digital quantitation and point grid counting of cardiac fibrous tissue.[8] The difference is possibly a result of thinly occupied areas of fibrous tissue tending to be regarded as fibrous tissue in the point grid quantitation, whereas in the digital quantitation they may be mostly ECP. Point grid counting has been used for similar purposes in previous studies.[8,9]

It is recognized that digital quantitation of the VG-stained microsections instead of point grid counting may have served the purpose of verifying the autofluorescence-based quantitation more appropriately. Indeed, we attempted to develop a color deconvolution algorithm for quantifying the VG-stained tissue components. However, vigorous image manipulation to the point of hardly recognizable tissue with considerable loss of detail was necessary. The attempt was eventually deemed a failure and point grid counting was selected for verification of the autofluorescence based quantitation. Along with the analytical verification, this approach was considered sufficient.

Analytical verification of the quantitation of fibrous tissue and ECP was included because autofluorescence as presented is relatively unexplored in the context of digital quantitation. Thus, a rational approach in addition to the point grid counting was considered necessary to exclude a coincidental correlation between the point grid counting and the digital quantitation.

The unknown fixation time is an issue that deserves discussion. Fixation time is a known parameter of relevance to autofluorescence intensity in that autofluorescence increases with fixation time.[15] In the current study, the quantitation was based on relative differences in the autofluorescence intensities of different tissue components. It was reported that increase in autofluorescence with fixation time was accompanied by only small changes in the autofluorescence spectrum,[15] which indicates an even autofluorescence increase regardless of the tissue component. In the additional study evaluating fixation time, the method was applied successfully and validated with point grid counting on microsections from samples fixated for 1 and 4 days. Within the limited scope of the study, fixation time was of no apparent significance. We recommend using fixation times between 1 and 4 days.

It is recognized that variation in microsection thickness cannot be avoided. The quantitation algorithms are based on intrasection parametric data analysis. Assuming a linear relationship between section thickness and autofluorescence intensity, this can be regarded as a shelter against bias. This linear relationship, however, has not been established. In the additional study evaluating microsection thickness, the method was applied successfully and validated with point grid counting on microsections cut at 2 and 8 μm. Autofluorescence intensity increased with microsection thickness. The study, however, was too small to establish the detailed relationship between microsection thickness and autofluorescence intensity. It was noted that thick microsections resulted in unclear borders between tissue components in the VG-staining and less obvious correspondence between the digital quantitations and VG-staining. It is recommended to use uniformly thin microsections.

Bleaching of the slides during handling, i.e., destruction of fluorescence resulting from light exposure, is a possible source of bias. Slides were handled identically and with minimal exposure to light, thereby minimizing a potential bleaching effect. As a part of the scanning process, the slide scanner automatically sets the focus guided by a prescan identification of the focus plane in selected tiles. When using the RAC-mode for autofocus, no bleaching could be detected digitally, whereas when using fluorescence-based autofocus, clear bleaching was seen in the autofocus tiles. RAC-mode was used to avoid bleached tiles, which would otherwise have to be omitted from the analysis.

The slide scanner used was mounted with an LED illumination source, which produces an excitation beam of more uniform wavelength as compared to traditional illumination sources. This is considered an advantage in that a narrow-banded excitation beam is more likely to produce autofluorescence contrast resulting in images suitable for analysis.

The presented method could be valuable in diagnosing arrhythmogenic right ventricle cardiomyopathy, which requires quantitation of fibrous tissue.[17] Cardiomyopathy research may benefit from the method considering the increasing evidence that fibrous tissue presence is a marker of severity[18,19] and distribution a marker of the phenotype.[14,20] The method may be applicable in other organs of interest, for example, when quantitating fibrosis in kidney or liver. In addition, the accurate digital outlines of tissue components may provide a framework for the digital analysis of stainings performed after the autofluorescence analysis, for instance of immunohistological stains.

CONCLUSION

We have shown that autofluorescence intensity of unstained microsections may provide ample contrast to quantitate and outline multiple components in cardiac tissue. The quantitations are considered verified with a comparison to point grid counting. Quantitative analysis of autofluorescence may prove useful in the diagnosis of cardiomyopathies and other areas of histology, for example, in analyzing fibrosis in hepatic or renal tissue. The perspectives, however, of a fully automated histological multicomponent quantitation and outlining tool based on unstained microsections are best appreciated in a digital light-an optimistic view sees quantitative autofluorescence analysis as the prestain starting point of any digital microscopy evaluation, providing a digital framework for image analysis of the staining to come.

Acknowledgment

The study was performed without external funding. The authors are grateful to Jasna Tahirovic and Heidi

Ugleholdt at the Department of Pathology, Rigshospitalet, and Anett Wollesen at the Department of Forensic Pathology, University of Copenhagen for invaluable help.

Financial Support and Sponsorship
Nil.

Conflicts of Interest
There are no conflicts of interest.

REFERENCES

1. Moran C, Münch G, Forbes JM, Beare R, Blizzard L, Venn AJ, *et al.* Type 2 diabetes, skin autofluorescence, and brain atrophy. Diabetes 2015;64:279-83.
2. Renkoski TE, Banerjee B, Graves LR, Rial NS, Reid SA, Tsikitis VL, *et al.* Ratio images and ultraviolet C excitation in autofluorescence imaging of neoplasms of the human colon. J Biomed Opt 2013;18:16005.
3. Schueth A, van Zandvoort MA, Buurman WA, van Koeveringe GA. Murine bladder imaging by 2-photon microscopy: An experimental study of morphology. J Urol 2014;192:973-80.
4. Thekkek N, Richards-Kortum R. Optical imaging for cervical cancer detection: Solutions for a continuing global problem. Nat Rev Cancer 2008;8:725-31.
5. Croce AC, De Simone U, Freitas I, Boncompagni E, Neri D, Cillo U, *et al.* Human liver autofluorescence: An intrinsic tissue parameter discriminating normal and diseased conditions. Lasers Surg Med 2010;42:371-8.
6. Prabhu V, Rao SB, Fernandes EM, Rao AC, Prasad K, Mahato KK. Objective assessment of endogenous collagen *in vivo* during tissue repair by laser induced fluorescence. PLoS One 2014;9:e98609.
7. Caorsi V, Toepfer C, Sikkel MB, Lyon AR, MacLeod K, Ferenczi MA. Non-linear optical microscopy sheds light on cardiovascular disease. PLoS One 2013;8:e56136.
8. Daunoravicius D, Besusparis J, Zurauskas E, Laurinaviciene A, Bironaite D, Pankuweit S, *et al.* Quantification of myocardial fibrosis by digital image analysis and interactive stereology. Diagn Pathol 2014;9:114.
9. Hadi AM, Mouchaers KT, Schalij I, Grunberg K, Meijer GA, Vonk-Noordegraaf A, *et al.* Rapid quantification of myocardial fibrosis: A new macro-based automated analysis. Cell Oncol (Dordr) 2011;34:343-54.
10. Ikeda H, Tauchi H, Shimasaki H, Ueta N, Sato T. Age and organ difference in amount and distribution of autofluorescent granules in rats. Mech Ageing Dev 1985;31:139-46.
11. Martin TP, Norris G, McConnell G, Currie S. A novel approach for assessing cardiac fibrosis using label-free second harmonic generation. Int J Cardiovasc Imaging 2013;29:1733-40.
12. Pickering JG, Boughner DR. Fibrosis in the transplanted heart and its relation to donor ischemic time. Assessment with polarized light microscopy and digital image analysis. Circulation 1990;81:949-58.
13. Tohma H, Hepworth AR, Shavlakadze T, Grounds MD, Arthur PG. Quantification of ceroid and lipofuscin in skeletal muscle. J Histochem Cytochem 2011;59:769-79.
14. Gho JM, van Es R, Stathonikos N, Harakalova M, te Rijdt WP, Suurmeijer AJ, *et al.* High resolution systematic digital histological quantification of cardiac fibrosis and adipose tissue in phospholamban p.Arg14del mutation associated cardiomyopathy. PLoS One 2014;9:e94820.
15. Xu MG, Williams ED, Thompson EW, Gu M. Effect of handling and fixation processes on fluorescence spectroscopy of mouse skeletal muscles under two-photon excitation. Appl Opt 2000;39:6312-7.
16. Schneider CA, Rasband WS, Eliceiri KW. NIH Image to ImageJ: 25 years of image analysis. Nat Methods 2012;9:671-5.
17. Marcus FI, McKenna WJ, Sherrill D, Basso C, Bauce B, Bluemke DA, *et al.* Diagnosis of arrhythmogenic right ventricular cardiomyopathy/dysplasia: Proposed modification of the task force criteria. Circulation 2010;121:1533-41.
18. Arteaga E, de Araújo AQ, Bernstein M, Ramires FJ, Ianni BM, Fernandes F, *et al.* Prognostic value of the collagen volume fraction in hypertrophic cardiomyopathy. Arq Bras Cardiol 2009;92:210-4, 216-20.
19. O'Hanlon R, Grasso A, Roughton M, Moon JC, Clark S, Wage R, *et al.* Prognostic significance of myocardial fibrosis in hypertrophic cardiomyopathy. J Am Coll Cardiol 2010;56:867-74.
20. Sepehrkhouy S, Gho J, Van Es R, Harakalova M, De Jonge N, Van Der Smagt J, *et al.* The Distribution Pattern of Fibrosis in Genetic Cardiomyopathy is Related to the Type of Pathogenic Mutation. 6th Biennial Meeting of the Association for European Cardiovascular Pathology; 2014.